Theoretical studies on the dispersion of the nonlinear optical susceptibilities in GaAs, InAs, and InSb†

C. Y. Fong*
Department of Physics, University of California, Davis, California 95616

Y. R. Shen‡
Department of Physics, University of California, Berkeley, California 94720
and Inorganic Material Research Division, Lawrence Berkeley Laboratory, Berkeley, California 94720

(Received 27 March 1975)

The nonlinear optical susceptibilities, $|\chi_{14}^{(2)}(2\omega)|$ for second-harmonic generation of GaAs, InAs, and InSb in the range $0.05 \leq \hbar\omega \leq 3.0$ eV are calculated from the band structure obtained by the empirical pseudopotential method. The spin-orbit interaction has been taken into account, and the transitions from the top four valence bands to the bottom four conduction bands are included in the calculation. The calculated $|\chi_{14}^{(2)}(2\omega)|$ with the $\vec{k}$-dependent dipole matrix elements give much better agreement with the available experimental data than the results of constant matrix elements, which, in turn, show more structure than the ones calculated by Bell. In the case of InSb, there are two structures at 1.6 and 1.8 eV due to double resonances. A simplified model to predict structure in $|\chi_{14}^{(2)}(2\omega)|$ from the linear spectrum is discussed.

I. INTRODUCTION

Experiments on the dispersion of the nonlinear optical susceptibilities, $|\chi_{14}^{(2)}(2\omega)|$, of zinc-blende semiconductors were first carried out by Chang *et al.*[1] Their results indicated that it is possible to correlate the structures in $|\chi_{14}^{(2)}(2\omega)|$ with the band-structure effect. However, more systematic experimental results have become available only recently[2-4] with the advent of tunable dye lasers. A comparison between the experiment and the theory can now be made more meaningful.

The microscopic expression of $|\chi_{14}^{(2)}(2\omega)|$ can be obtained easily from second-order perturbation calculations.[5-9] It is seen that for solids, a complete understanding of the dispersion of $\chi^{(2)}(2\omega)$ requires detailed information of the energies and the wave functions of the electronic states in the first Brillouin zone (BZ). Since this information is not readily available, theoretical efforts have been directed to two cases: (a) finding the limiting values of $|\chi_{14}^{(2)}(2\omega)|$ as $\omega \to 0$ (ω well below the electronic transitions but above the vibrational transitions), and (b) obtaining a semiquantitative understanding of the dispersion of $\chi^{(2)}(2\omega)$ by simplifying approximations. In the first case, both the bond-charge model[10] and the charge-transfer model[11,12] derived from the valence-bond theory[13] have been very successful. However, the controversy of whether it is the bond-charge or the charge-transfer model that is responsible for $\chi^{(2)}(2\omega)$ has not yet been resolved. In the second case, Bloembergen *et al.*[14] showed that the structure in $\chi^{(2)}(2\omega)$ may be related to structure in the linear susceptibilities $\chi^{(1)}(\omega)$ and $\chi^{(1)}(2\omega)$. However, in their formalism, the possible double-resonance effect, which occurs when both ω and 2ω are near resonance at the same point in the Brillouin zone, is buried away. Recently, Bell[15] used a simplified three-band model to calculate $|\chi_{14}^{(2)}(2\omega)|$ for GaAs, InAs, InSb, and ZnTe in the range $0.05 \leq \hbar\omega \leq 2.0$ eV. He made the following assumptions in the calculations: (a) The structures in $|\chi^{(2)}(2\omega)|$ for $\hbar\omega \leq 2.0$ eV are entirely due to ω or 2ω resonances with the transitions between the top valence band and the two lowest conduction bands at the critical points of Γ and along Λ in the Brillouin zone. (b) The energy separations between the valence band and the first conduction band have a parabolic shape at Γ and a hyperbolic form with a two-dimensional minimum at Λ. The energy separation between the valence band and the second conduction band has a parabolic form at both Γ and Λ. (c) The transition matrix elements are constant and equal to the value evaluated at Γ. (d) All other transitions from the valence bands to the higher-energy conduction bands contribute to the smooth background in $|\chi_{14}^{(2)}(2\omega)|$. Using these simplifications, Bell was able to account for most of the previously observed structure in $\chi_{14}^{(2)}(2\omega)$. We shall discuss his results in more detail in later sections.

Except for that given by Bell, no other more realistic calculation of $\chi^{(2)}(2\omega)$ has appeared in the literature. The major difficulties come from the lack of detailed information about the band structure and the transition matrix elements. Recently, empirical-pseudopotential band calculations have been very successful in reproducing the experimental linear reflectivities of solids, in particular, the IV and III-V semiconductors.[16,17] The resulting band structure and momentum (transition) matrix elements can then be used for calculations of other properties. In this paper, we report calculations of $|\chi_{14}^{(2)}(2\omega)|$ with $0.05 \leq \hbar\omega \leq 3.0$ eV for

GaAs, InAs, and InSb, using the energies and the transition matrix elements directly obtained from the empirical-pseudopotential band calculations. These results, we believe, represent the most realistic treatment on the dispersion of $|\chi_{14}^{(2)}(2\omega)|$ up to now. A brief discussion on the method of calculations will be given in Sec. II. In Sec. III, we shall present the results of our calculations with and without the assumption of constant matrix element. We shall then compare our results with those of Bell[15] and also with the available experimental data. In Sec. IV, we shall discuss the limiting values of $|\chi_{14}^{(2)}(2\omega)|$ as $\omega \to 0$ for the three compounds, and present a simple model for understanding and predicting the semiquantitative features of $\chi^{(2)}(2\omega)$ from the linear spectrum. Finally, a brief summary is given in Sec. V.

II. METHOD OF CALCULATIONS

In the crystals with zinc-blende structures, the second-order nonlinear optical susceptibility can be written as[7,15,18]

$$\chi_{14}^{(2)}(2\omega) = \tfrac{1}{2}\sqrt{3}\,\chi_{[111]}^{(2)}(2\omega), \tag{1}$$

where $\chi_{[111]}^{(2)}$ is the susceptibility with the electric field and the induced-dipole moment in the [111] direction; the explicit expression of $\chi_{[111]}^{(2)}(2\omega)$ normalized in a unit volume is given by

$$\chi_{[111]}^{(2)}(2\omega) = -\frac{e^3}{2m^3\omega^3}\sum_{\vec{k}}\sum_{v,c,c'} P_{vc}^{[111]}(\vec{k})\,P_{cc'}^{[111]}(\vec{k})\,P_{c'v}^{[111]}(\vec{k})\,f_v(\vec{k})$$
$$\times\left(\frac{1}{[E_{cv}(\vec{k})-2\hbar\omega)][E_{c'v}(\vec{k})-\hbar\omega]}+\frac{1}{[E_{cv}(\vec{k})-\hbar\omega][E_{c'v}(\vec{k})+\hbar\omega]}\,\frac{1}{[E_{cv}(\vec{k})+\hbar\omega][E_{c'v}(\vec{k})+2\hbar\omega]}\right), \tag{2}$$

where $E_{cv}(\vec{k})$ is the interband energy between the conduction-band state $|c,\vec{k}\rangle$ and the valence-band state $|v,\vec{k}\rangle$, and $P_{cv}^{[111]}(\vec{k})$ is the corresponding momentum matrix element along the [111] direction. In terms of the Cartesian components along the three [100] directions, $P_{cv}^{[111]}(\vec{k})$ is expressed as

$$P_{cv}^{[111]} = (P_{cv}^{x} + P_{cv}^{y} + P_{cv}^{z})/\sqrt{3}. \tag{3}$$

The product of the matrix elements in Eq. (2) leads to the fact that at each $\vec{k}$ point, the contribution to $\chi^{(2)}(2\omega)$ has to involve three states. However, the Fermi-Dirac functions, $f_v(\vec{k})$, restricts the transitions from one valence band to two conduction bands The obvious $1/\omega^3$ divergence in Eq. (2) does not present difficulty in the actual determination of $\chi_{[111]}^{(2)}(2\omega)$, as has been discussed in detail by Aspnes.[18]

We calculate $|\chi_{14}^{(2)}(2\omega)|$ directly from Eq. (2) using the interband energies and the momentum matrix elements obtained from the empirical-pseudopotential band-structure calculations.[17,18] The spin-orbit (SO) interaction has been taken into account in these calculations. At present, the only available experimental data appear in the range $\hbar\omega \leq 3.0$ eV, so we include only transitions from the four top valence bands to the four bottom conduction bands. In the momentum matrix elements, the SO term is neglected because it is several orders of magnitude smaller than the contribution of $\langle c\vec{k}|\vec{p}|v\vec{k}\rangle$. The integration over $\vec{k}$ space is performed by a linear interpolation scheme.[19] By symmetry, we only have to integrate over $\frac{1}{48}$ of the BZ. The interband energies and the product of the matrix elements are calculated at 152 mesh points in this $\frac{1}{48}$ part of the BZ. Approximately 9.3×10^5 sampling points are generated by a Monte Carlo method. The interband energies and the matrix elements associated with each random point are obtained by linearly interpolating between the points on the mesh. A phenomenological damping constant of 0.05 eV is introduced in the energy denominators of Eq. (2). We use frequency intervals of 0.05 eV for $\hbar\omega \leq 2.0$ eV, and 0.1 eV for $2.0 \leq \hbar\omega \leq 3.0$ eV.

We have also calculated $|\chi_{14}^{(2)}(2\omega)|$ with constant momentum matrix elements for the three crystals, so that a comparison with Bell's results can be made and the importance of including the actual matrix elements in the calculations can be evident.

III. RESULTS

Although the three crystals have the same zinc-blende structure, there are detailed differences in their electronic properties; for example, their fundamental gaps have different values. It is, therefore, more convenient to discuss the results for each crystal separately. We shall start with GaAs, then InAs, and finally InSb. For the first two cases, we shall first present the result of constant matrix elements $|\chi_{14}^{(2)}(2\omega)|$ and compare it with Bell's calculation. The $|\chi_{14}^{(2)}(2\omega)|$ with $\vec{k}$-dependent matrix elements is then compared with the one with constant matrix elements and with the experimental results. For InSb, we shall also point out some difficulties involved and the occurrence of double resonances in the calculation.

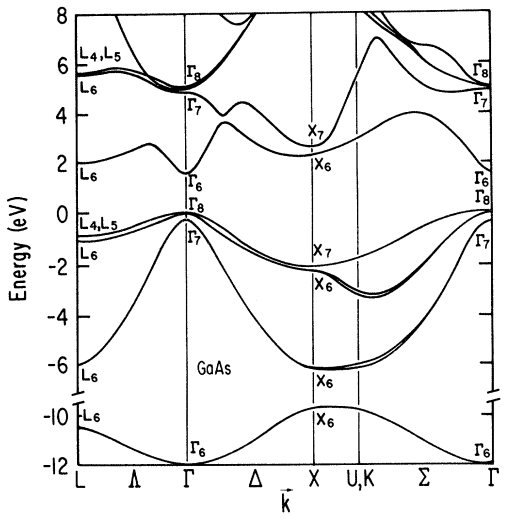

FIG. 1. Band structure of GaAs.

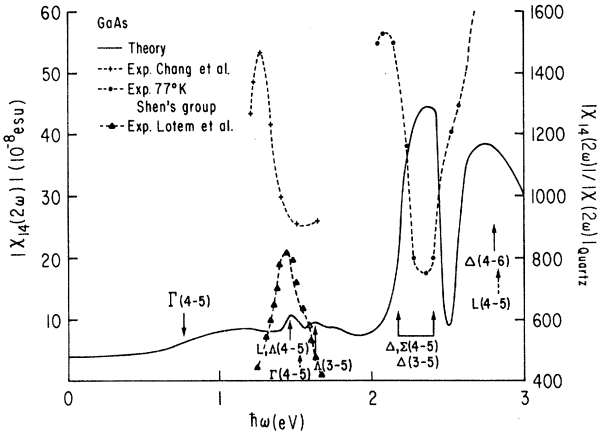

FIG. 3. Comparison of $|\chi_{14}^{(2)}(2\omega)|$ of GaAs with available experimental data.

A. GaAs

The band structure of GaAs used for the present calculation of $|\chi_{14}^{(2)}(2\omega)|$ was obtained by fitting to the measured logarithmic derivatives of the reflectivity.[16] It is reproduced in Fig. 1, and is used as a prototype band structure for the three compounds. The linear optical spectrum obtained from this band structure agrees with the experimental spectrum to about 0.1 eV for $0 \leq \hbar\omega \leq 5.0$ eV. The important critical points (CPs) associated with the structure in the linear spectrum are given in Table I, because they also contribute significantly to the nonlinear optical spectrum. As seen from Eq. (2), we expect $\chi_{14}^{(2)}(2\omega)$ to show structure when either ω or 2ω or both are at resonance with critical-point transitions.

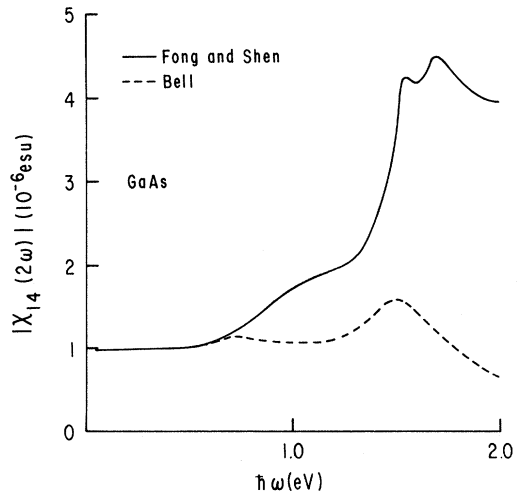

FIG. 2. Comparison of the constant matrix element $|\chi_{14}^{(2)}(2\omega)|$ of GaAs with Bell's calculations (Ref. 15).

In Fig. 2, $|\chi_{14}^{(2)}(2\omega)|$ of GaAs with constant momentum matrix elements for $0.05 \leq \hbar\omega \leq 2.0$ eV, is shown in solid line and is normalized to the results obtained by Bell (shown in dashed line) at 0.05 eV. This normalization is purely for convenience in comparing the two results. The values of $|\chi_{14}^{(2)}(2\omega)|$ of Ref. 15 at 0.05 eV are questionable because of a possible error in the numerical factor of the expression[18] of $\chi_{14}^{(2)}(0)$. From Table I, we would expect to see structure in $|\chi_{14}^{(2)}(2\omega)|$ at 0.76, 1.52, and 1.63 eV for $\hbar\omega \leq 2.0$ eV due to either ω or 2ω at resonance with the E_0 and E_1 peaks. As shown in Fig. 2, however, the expected structure at 0.76 eV is smeared out by contributions from other transitions, especially along Δ (see Fig. 1), because of the small density of states at Γ (for E_0). We do find peaks at 1.50 and 1.65 eV that can be attributed to the ω resonance with the fundamental gap at Γ (E_0 peak) and the 2ω resonance with the SO split peaks (E_1) of the $\Lambda(3-5, 4-5)$ transitions. The SO effect Δ_0 at $\Gamma(2-5)$ has not been included in our calculations. The dashed curve by Bell, however, shows peaks at 0.75 and 1.5 eV. The magnitude of the dashed curve is, in general, smaller than the solid curve. This is also true in InAs and InSb, as we shall see. The differences arise from Bell's approximations. As we mentioned earlier, Bell has approximated the band structure by a three-band model which has two conduction bands and one valence band with only two critical points at $\vec{k}=0$ (Γ) and $\vec{k}=\frac{2}{3}(1,1,1)\pi/a$ (along Λ), respectively, where a is the lattice constant. Therefore, his results of $|\chi_{14}^{(2)}(2\omega)|$ should have a weaker background. Furthermore, it explains why the structure at 0.75 eV shown in the dashed curve is more prominent. The ex-

TABLE I. Critical points associated with the structure in the linear calculated reflectivity of GaAs.

Reflectivity structure		Associated critical points			
Theory		Location in zone		Symmetry	CP energy (eV)
1.52 eV	E_0	$\Gamma(4-5)$	(0,0,0)	M_0	1.52
2.90	E_1	$L(4-5)$	(0.5,0.5,0.5)	M_0	2.82
		$\Lambda(4-5)$	(0.2,0.2,0.2)	M_1	3.02
3.25	$E_1+\Delta_1$	$\Lambda(3-5)$	(0.2,0.2,0.2)	M_1	3.25
		$\Delta(4-5)$	(0.6,0,0)	M_0	4.23
		$\Delta(3-5)$	(0.6,0,0)	M_0	4.36
4.92	E_2	$\Delta(4-5)$	(0.2,0,0)	M_1	4.38
		$\Delta(3-5)$	(0.2,0,0)	M_1	4.55
		$\Sigma(4-5)$	(0.6,0.6,0)	M_2	4.88
		$\Delta(4-6)$	(0.5,0,0)	M_1	5.67
		$\Delta(3-6)$	(0.5,0,0)	M_1	5.81

pected spin-orbit splitting of the 1.5-eV peak is missing in Bell's curve.

The curve of $|\chi_{14}^{(2)}(2\omega)|$ of GaAs with $\vec{k}$-dependent momentum matrix elements is given in Fig. 3 for the range $0.05 \leq \hbar\omega \leq 3.0$ eV. The peaks originating from 2ω resonance around the critical points are marked by solid arrows, whereas the ones from ω resonance around the critical points are marked by dashed arrows. On the same graph, we also show three different sets of experimental results.[2-4] The results of Parsons and Chang[2] cover the range 1.1–1.7 eV, those of Lotem *et al.*[3] cover 1.2–1.8 eV, and the results of Bethune *et al.*[4] cover $1.95 \leq \hbar\omega \leq 2.7$ eV. The signals measured in Ref. 2 were relative to ammonium dihydrogen phosphate (ADP), whereas those in Refs. 3 and 4 were relative to quartz.

Similar to the case of constant matrix elements, the 0.76-eV structure is smeared out by the nearby-energy transitions. The twin structure between 1.4 and 1.7 eV which also appears in Fig. 2 is due to the 2ω resonance with the spin-orbit split of the E_1 peaks. The matrix elements enhance the $\Lambda(4-5)$ transitions; therefore, the relative magnitudes of the two peaks are reversed in Figs. 2 and 3. The ω resonance of the $\Gamma(4-5)$ transitions provide only the background to the 1.45-eV peak in Fig. 3.

The experimental results of Ref. 2 show a single peak at 1.26 eV which is 0.19 eV lower than the theoretical value at 1.45 eV. Lotem *et al.*,[3] however, found a peak at 1.44 eV and a shoulder at 1.55 eV in their work, as seen in Fig. 3; both the positions and the general shapes of the structure agree well with the theoretical curve, except that the experimental peak is broader. This peak was suggested by Lotem *et al.*[3] as due to ω resonance with the E_0 peak. We believe that their assignment cannot be true since the density of state associated with the E_0 peak is small.

In the higher-frequency range, if the experimental curve of Bethune *et al.*[4] was shifted up in energy by about 0.2 eV, theory and experiment would be in good agreement. This discrepancy is somewhat similar to the case of Ref. 2 in the low-energy region. In other words, the critical-point energies that are extracted from $|\chi_{14}^{(2)}(2\omega)|$ appear to be 0.2 eV lower than those determined from the linear spectrum. It is believed that the shifts may be due to laser heating of the sample surface.[4] We can assign the theoretical peak at 2.35 eV to 2ω resonance with Δ, $\Sigma(4-5)$ and $\Delta(3-5)$ transitions. These transitions give rise to the main peak (E_2 peak) at 4.8 eV in the linear spectrum. A large volume effect in the Brillouin zone near Δ and Σ provides the huge background to this E_2 peak. Therefore, the intensity of the 2.35-eV peak in $|\chi_{14}^{(2)}(2\omega)|$ is about four times larger than the ones around 1.4–1.7 eV contributed by the E_1 peak. The theoretical

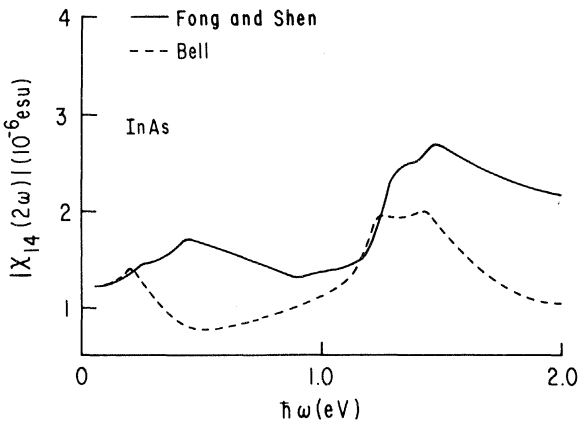

FIG. 4. Comparison of the constant matrix element $|\chi_{14}^{(2)}(2\omega)|$ of InAs with Bell's calculations (Ref. 15).

TABLE II. Summary of the experimental and theoretical structure in $|\chi_{14}^{(2)}(2\omega)|$ of GaAs.

Structure in $\lvert\chi_{14}^{(2)}(2\omega)\rvert$ in terms of peaks in linear optical spectrum	Experiment			Theory		
	Parsons and Chang (Ref. 2)	Lotem Koren, and Yacoby (Ref. 3)	Bethune, Schmidt, and Shen (Ref. 4)	Bell (Ref. 15)	Fong and Shen (constant matrix element)	Fong and Shen ($\vec{k}$-dependent matrix element)
$\frac{1}{2}-E_0$ $\frac{1}{2}-E_0+\Delta_0$				0.75 eV	smeared out	smeared out
E_0		1.43 eV (background)		1.5	1.52 eV	1.52 eV (background)
$E_0+\Delta_0$						
$\frac{1}{2}-E_1$	1.26 eV	1.44 (peak)			1.5	1.45 (peak)
$\frac{1}{2}-E_1+\Delta_1$		1.55 (shoulder)		1.5	1.65	1.60 (weak peak)
E_1						2.80
$\frac{1}{2}-E_2$			2.1 eV (peak) 2.5 (shoulder)			2.35 (peak) 2.75 (broad weaker peak)

peak around 2.75 eV arises from ω resonance with $\Lambda(4-5)$ transitions and 2ω resonance with $\Lambda(3, 4-6)$ transitions. We note that in the linear spectrum, the contribution from the 3–5 and 4–5 transitions and that from the 3–6 and 4–6 transitions lead to one broad E_2 peak around 5 eV, but in the nonlinear $\chi^{(2)}(2\omega)$ spectrum, they actually lead to two separate peaks at 2.35 and 2.75 eV. A summary of comparison between the experimental and theoretical results is given in Table II.

B. InAs

The band structure of InAs is similar to that of GaAs given in Fig. 1. A list of critical points in the linear optical transitions is given in Table III. In Fig. 4, the present calculation of $|\chi_{14}^{(2)}(2\omega)|$ with constant matrix elements is compared with the result of Bell. In the low-energy region ($\hbar\omega < 0.5$ eV), the solid curve from our calculations shows two structures at 0.25 and 0.45 eV. They correspond, respectively, to 2ω and ω resonance with the fundamental gap (E_0 peak). The 0.25-eV peak has not been smeared out because, unlike the case of GaAs, the slope of E vs $\vec{k}$ near Γ along Δ in InAs is considerably large. The dashed curve of Bell shows only one peak, at 0.2 eV. The agreement between the two curves in the 1–2-eV range is much better. Our calculations give two peaks,

TABLE III. Critical points associated with the structure in the linear calculated reflectivity of InAs.

Reflectivity structure		Associated critical points (InAs)		
Theory		Location in zone	Symmetry	CP energy (eV)
0.46 eV	E_0	$\Gamma(4-5)$ (0, 0, 0)	M_0	0.46
2.58	E_1	$\Lambda(4-5)$ (0.3, 0.3, 0.3)	M_1	2.47
		$L(4-5)$ (0.5, 0.5, 0.5)	M_1	2.48
2.85	$E_1+\Delta_1$	$\Lambda(3-5)$ (0.3, 0.3, 0.3)	M_1	2.74
		$L(3-5)$ (0.5, 0.5, 0.5)	M_1	2.75
		$\Delta(4-5)$ (0.7, 0, 0)	M_1	4.3
		$\Gamma(4-6)$ (0, 0, 0)	···	4.37
		$X(4-5)$ (1.0, 0, 0)	M_1	4.43
		Vol. near (3–5) (0.7, 0, 0)	···	4.43
4.68	E_2	$\Sigma(4-5)$ (0.7, 0.7, 0)	M_2	4.65
		$\Delta(3-6)$ (0.3, 0, 0)	M_1	4.69
		Vol. near $\Delta(4-5)$ (0.7, 0, 0)	···	5.25
		Vol. near $\Delta(3-6)$ (0.7, 0, 0)	···	5.39

TABLE IV. Summary of the experimental and the theoretical structure in $|\chi_{14}^{(2)}(2\omega)|$ of InAs.

Structure in $\lvert\chi_{14}^{(2)}(2\omega)\rvert$ in terms of peaks in the linear optical spectrum	Experiment: Parsons and Chang (Ref. 2)	Experiment: Bethune, Schmidt, and Shen (Ref. 3)	Theory: Bell (Ref. 15)	Theory: Fong and Shen (constant matrix element)	Theory: Fong and Shen ($\vec{k}$-dependent matrix element)
$\frac{1}{2}-E_0$			0.2 eV	0.25 eV	0.3 eV
E_0				0.45	0.45
$\frac{1}{2}-E_1$	1.25 eV		1.25	1.3	1.3
$\frac{1}{2}-E_1+\Delta_1$	1.4		1.42	1.45	1.45
E_1		2.5 eV			2.6
$E_1+\Delta_1$		(shoulder)			(shoulder)
$\frac{1}{2}-E_2$		2.28			2.3

at 1.3 and 1.45 eV, arising from the 2ω resonance with the E_1 and $E_1+\Delta_1$ SO split peaks. Bell's calculations, assuming E_1 and $E_1+\Delta_1$ at 2.5 and 2.78 eV, respectively, give the corresponding peaks at 1.25 and 1.42 eV. Owing to the reason discussed in Sec. III A, the solid curve is generally larger in magnitude than the dashed one.

The calculated $|\chi_{14}^{(2)}(2\omega)|$ of InAs with the $\vec{k}$-dependent matrix elements is shown in Fig. 5 with the origins of the structures marked. As discussed earlier, the two peaks at 0.3 and 0.45 eV are due to 2ω and ω resonances with the E_0 peak, respectively. The $\vec{k}$-dependent matrix elements do not shift the peaks at 1.3 and 1.45 eV due to 2ω resonances with the E_1 and $E_1+\Delta_1$ peaks, but they do have an influence on the magnitudes of the peaks. Comparison between Figs. 4 and 5 shows that the relative strengths of the peaks have been inverted. The experimental results of Parsons and Chang[2] in this frequency range, also shown in Fig. 5, are in good agreement with the calculated curve, both in the position of the peaks and in the relative strengths of the peaks.

In the higher-energy region, the calculated $|\chi_{14}^{(2)}(2\omega)|$ in Fig. 5 shows a broad peak at energy between 2.3 and 2.6 eV. This is due to 2ω resonances with the E_2 peak arising from $\Delta, X, \Sigma(4-5)$ transitions. The ω resonances with the E_1 and $E_1+\Delta_1$ peaks also contribute to the 2.6-eV region of this broad structure. The measured results in Ref. 4 show a peak at 2.28 eV and a broad shoulder at about 2.5 eV, in fair agreement with the theo-

TABLE V. The critical points associated with the structure in the linear calculated reflectivity of InSb.

Reflectivity structure: Theory		Associated critical points (InSb): Location in Zone	Symmetry	CP energy (eV)
0.26 eV	E_0	$\Gamma(4-5)$ (0, 0, 0)	M_0	0.26
2.03	E_1	$\Lambda(4-5)$ (0.3, 0.3, 0.3)	M_1	1.94
		$L(4-5)$ (0.5, 0.5, 0.5)	M_1	2.0
2.60	$E_1+\Delta_1$	$\Lambda(3-5)$ (0.3, 0.3, 0.3)	M_1	2.5
		$L(3-5)$ (0.5, 0.5, 0.5)	M_1	2.55
		$\Delta(4-5)$ (0.7, 0, 0)	M_1	3.65
		$\Delta(3-5)$ (0.7, 0, 0)	M_1	3.83
		$\Delta(3-6)$ (0.2, 0, 0)	M_1	3.95
		$\Sigma(4-5)$ (0.7, 0.7, 0)	M_2	4.1
		Vol. near $\Delta(4-6)$ (0.5, 0, 0)	···	4.4
		$\Delta(4-6)$ (0.7, 0, 0)	M_3	4.75
4.1	E_2	$L(4-6)$ (0.5, 0.5, 0.5)	M_0	4.86
		$\Lambda(4-6)$ (0.4, 0.4, 0.4)	M_1	4.87
		$\Delta(3-6)$ (0.7, 0, 0)	M_3	4.94
		$L(3-6)$ (0.5, 0.5, 0.5)	M_0	5.41
		$\Lambda(3-6)$ (0.4, 0.4, 0.4)	M_1	5.43

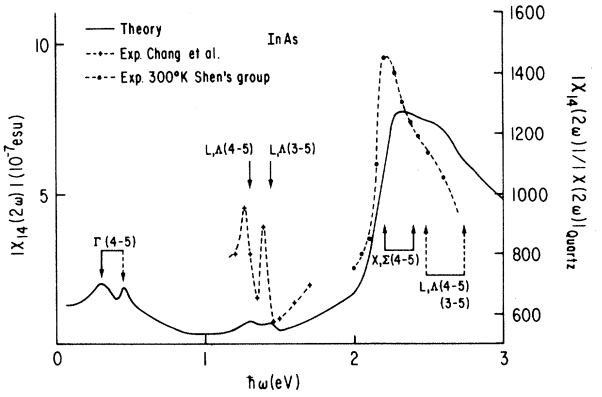

FIG. 5. Comparison of $|\chi_{14}^{(2)}(2\omega)|$ of InAs with available experimental data.

retical calculations. In Table IV, we summarize the comparison.

C. InSb

There are several difficulties in calculating the nonlinear optical properties of InSb as compared with the other two cases. First, the available band structure of InSb is not as accurate as those of GaAs and InAs. We have used the pseudopotential parameters given by deAlvarez *et al.*[17] In order to reproduce their interband energies at the critical points listed in Table V, it is necessary to use the value of 0.002 37 Ry for the parameter characterizing the SO interaction of the metallic ion, instead of 0.002 03 Ry given by deAlvarez *et al.*[17] Second, the quality of the calculated optical spectrum of InSb appears to be more strongly affected by the mesh size used in the calculation. We have used a mesh of 152 points as compared to 356 points used by deAlvarez *et al.* Our $\epsilon_2(\omega)$ spectrum in the range $0.5 \leq \hbar\omega \leq 1.5$ eV shows more fluctuation than theirs. We also obtain a weak peak at 1.8 eV; they found a hump. This structure has not been observed experimentally, and it arises presumably from inaccuracy of the band structure. Finally, occurrence of possible double resonances complicates the $|\chi_{14}^{(2)}(2\omega)|$ spectrum. There are two local regions where the energies of the 4–6 transitions are twice those of the 4–5 transitions: (i) a small region in the ΓKX plane near Γ (about $\frac{1}{5}$ of ΓX), with transition energies around 3.2 and 1.6 eV, and (ii) a larger region around the ΓLK plane near Γ with transition around 3.6 and 1.8 eV.

The $|\chi_{14}^{(2)}(2\omega)|$ with constant matrix elements is plotted as the solid curve in Fig. 6. The two structures at 0.15 and 0.25 eV are due to ω and 2ω resonances with the fundamental gap (0.26 eV). A shoulder at 0.9 eV arises from the 2ω resonance with the spurious structure at 1.8 eV in the $\epsilon_2(\omega)$, as discussed earlier. The peaks at 1.05 and 1.35 eV are due to the 2ω resonances with the Λ-L critical-point transitions at 2.03 and 2.6 eV (E_1 peaks). A weak shoulder at $1.6 \leq \hbar\omega \leq 1.7$ eV is the result of double resonance (i), discussed earlier. Finally, the shoulder at 1.95 eV and the broad peak at 2.3 eV come from 2ω resonance with the broad E_2 peak and also partly from ω resonance with the E_1 peaks (Table V). The curve also shows a sharp dip at 1.8 eV. However, as we mentioned earlier, there is a peak at 1.8 eV in the calculated linear spectrum. One would therefore expect to find a peak instead of a dip at this energy. To understand this puzzling result, we have performed a calculation of $|\chi_{14}^{(2)}(2\omega)|$ with the product of the matrix elements taken as a constant but with the correct sign as obtained from the $\vec{k}$-dependent matrix elements. The result shows a strong peak at 1.8 eV. Apparently, in this case, the matrix elements are important because the double-resonance contribution can interfere strongly with the background either constructively or destructively, depending on the sign.

The result of Bell's calculation is also shown in Fig. 6 as the dashed curve. He assumed spin-orbit split E_0 peaks at 0.17 and 0.99 eV and the E_1 peaks at 1.88 and 2.38 eV. They give rise to the structures at 0.08, 0.45, 1.0, 1.24, and 1.88 eV in $|\chi_{14}^{(2)}(2\omega)|$. There is an obvious difference between the two curves in Fig. 6. In particular, Bell's curve shows a pronounced peak instead of a dip at 1.88 eV. This is because no interference due to double resonance can occur in his case, and he has assigned the lower E_1 peak at 1.88 eV.

The calculated $|\chi_{14}^{(2)}(2\omega)|$ with $\vec{k}$-dependent matrix elements is shown as the solid curve in Fig. 7. The identifications of the various transitions are labeled. The structure at 0.15 eV is due to 2ω resonance with the fundamental gap. The ω resonance with the fundamental and its SO split gaps

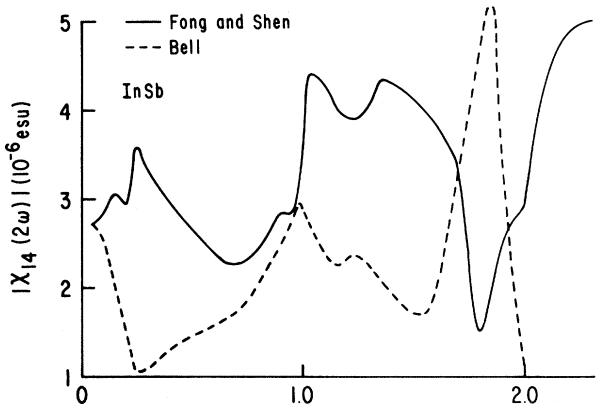

FIG. 6. Comparison of the constant matrix element $|\chi_{14}^{(2)}(2\omega)|$ of InSb with Bell's calculations (Ref. 15).

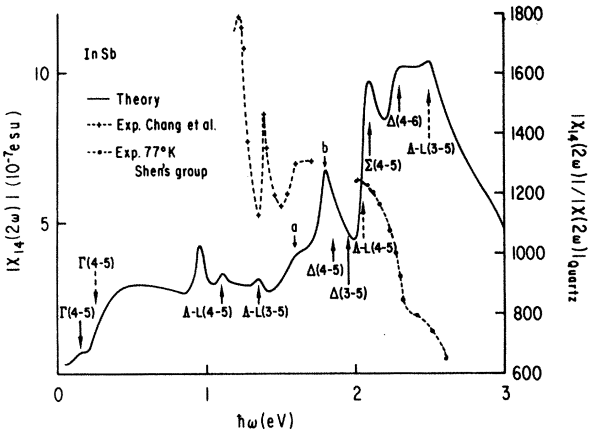

FIG. 7. Comparison of $|\chi_{14}^{(2)}(2\omega)|$ of InSb with available experimental data.

are masked out by the tail of higher-energy transitions. For $0.3 \leq \hbar\omega \leq 0.8$ eV, the calculated $|\chi_{14}^{(2)}(2\omega)|$ shows appreciable fluctuations which have been averaged out in Fig. 7. The shape in this region reflects the slope change[17] in the $\epsilon_2(\omega)$ near 0.8 eV. The structure at 0.95 eV is due to 2ω resonance with the 1.8-eV spurious peak in $\epsilon_2(\omega)$, discussed in Sec. III C. The peaks at 1.1 and 1.35 eV come from 2ω resonances with Λ-L (3–5, 4–5) transitions (E_1 peaks). The shoulder around 1.6 eV is due to double resonance (i), and the peak at 1.8 eV is due to double resonance (ii) and ω resonance with the 1.8-eV peak in $\epsilon_2(\omega)$. Of the three crystals that we have studied these double resonances happen only in InSb. The structures at $\hbar\omega \geq 2.0$ eV come from 2ω resonances with the critical points associated with the E_2 peak in the linear spectrum and ω resonances with the Λ-L transitions.

Comparison of the solid curves in Figs. 6 and 7 shows that there is a drastic difference at 1.8 eV. As we discussed earlier, the dip of the solid curve at 1.8 eV in Fig. 6 is due to incorrect signs of the matrix elements for the double-resonance term, leading to a destructive interference. Therefore, the $\vec{k}$-dependent matrix elements have significant effect on $|\chi_{14}^{(2)}(2\omega)|$. Furthermore, the strong dipole transition matrix elements associated with the $\Sigma(4-5)$ transitions split the broad peak at 2.3 eV for the constant matrix element case into two peaks at 2.1 and 2.3 eV, as shown in Fig. 7.

There exist three sets of experimental results for InSb. Wynne[20] measured $|\chi_{14}^{(2)}(2\omega)|_{InSb}/\chi_{14}^{(2)} \times(2\omega)|_{GaAs}$ for $\hbar\omega \leq 0.117$ eV, and observed a structure at 0.1167 eV. This structure corresponds to the one at 0.15 eV shown in Fig. 7. The small discrepancy is due to the limited resolution of the theoretical calculation. However, the ratio of the two susceptibilities calculated from Figs. 3 and 7 is less than 2, which is much smaller than the value of 12.2 given in Ref. 20. A possible reason is that the calculated dipole matrix elements of InSb are too small. Even in the linear case, the calculated reflectivity is about 20% lower than the experimental result for $\hbar\omega < 4$ eV.[17] The experimental result obtained by Parsons and Chang[2] in the frequency range $1.2 \leq \hbar\omega \leq 1.17$ eV is shown as the dashed curve in Fig. 7. It has two peaks at 1.22 and 1.38 eV and a shoulder at 1.65 eV. The first peak differs from the theoretical structure by 0.1 eV, and the other two structures show reasonable agreement. In particular, the shoulder at 1.65 eV suggests that double resonance (i) indeed occurs. It is unfortunate that experimental data are not available in the 1.8-eV region. Therefore, whether the strong double-resonance structure (ii) truly exists or it is simply the result of an imprecise band structure, remains to be answered. The data in the range $2.0 \leq \hbar\omega \leq 2.6$ eV measured by Bethune *et al.*[4] are shown as the dotted-dashed curve in Fig. 7. They observed two structures, at 2.2 and 2.4 eV, which are in rough agreement with the calculated ones, although the line shapes are quite different. A summary of the comparison between theory and experiments is given in Table VI.

IV. DISCUSSION

In the previous section, we discussed the dispersion of the nonlinear optical susceptibilities of three semiconductors. We shall now discuss our result for the limiting case where $\omega \to 0$, since there are several such measurements of $|\chi_{14}^{(2)}(2\omega)|$ for these compounds.[20] We shall also present in this section a simple model for calculating $|\chi_{14}^{(2)}(2\omega)|$ from the known $\epsilon_2(\omega)$ of the crystal.

As we see from Figs. 3, 5, and 7, the limiting values of the calculated $|\chi_{14}^{(2)}(2\omega)|$ are 4×10^{-8}, 1.25×10^{-7}, and 3×10^{-8} esu for GaAs, InAs, and InSb, respectively. Compared to the measured values[1,21] of 90 ± 30, 200 ± 60, and $300\pm150\times10^{-8}$ esu, the theoretical results are smaller by least one order of magnitude. To see whether these discrepancies can be due to the neglected higher-energy transitions, we have calculated the susceptibility of GaAs at 0.1 eV including two more valence and conduction bands, and found that the result was improved only by 10%. It is also unlikely that the matrix elements calculated from the pseudo wave functions can account for such a large difference. We feel that the lower theoretical values can be attributed to the local field effect. Although the three compounds are not insulators, the local field effect may not be completely neglected.[22] To support this speculation, we used the expression given by Bloembergen[23] to estimate the cor-

TABLE VI. Summary of the experimental and the theoretical structure in $|\chi_{14}^{(2)}(2\omega)|$ of InSb.

Structure in $\lvert\chi_{14}^{(2)}(2\omega)\rvert$ in terms of peaks in the linear optical spectrum and double resonances	Experiment		Theory		
	Parsons and Chang (Ref. 2)	Bethune, Schmidt, and Shen (Ref. 3)	Bell (Ref. 15)	Fong and Shen (constant matrix element)	Fong and Shen ($\vec{k}$-dependent matrix element)
$\frac{1}{2}-E_0$			0.08 eV	0.15 eV	0.15 eV
$\frac{1}{2}-E_0+\Delta_0$			0.45		
E_0				0.25	0.25
$E_0+\Delta_0$					(smeared out)
$\frac{1}{2}-E_1$	1.22 eV		1.0	1.05	1.1
$\frac{1}{2}-E_1+\Delta_1$	1.38		1.24	1.35	1.35
Double resonance *a*	1.65 (shoulder)			1.6 (shoulder)	1.6 (shoulder)
E_1		2.4 eV	1.88	2.3	2.05 (background)
$E_1+\Delta_1$					2.5
Double resonance *b*				1.8 (dip)	1.8
$\frac{1}{2}-E_2$		2.2		1.95 (shoulder)	2.1
					2.3
					2.5 (background)

rection. The three $\epsilon(\omega)$'s were approximated by averaged real and imaginary parts of the dielectric function in the frequency range $\hbar\omega \leq 6.0$ eV. The values for GaAs, InAs, and InSb are 11.4, 8.7, and 8.8, from the results of the empirical-pseudopotential calculation.[24] With the local-field correction, the limiting values of $|\chi_{14}^{(2)}(2\omega)|$ are 352, 565, and 140, respectively. Although the first two cases are now larger than the experimental data by about a factor of 2 and the value of InSb is still slightly smaller than the one given in Ref. 1 due to the weak matrix elements as we mentioned in Sec. III C, the result gives the correct order of magnitude. These corrections of the local-field effect are expected to be overestimated because the expression in Ref. 22 was derived for insulators.

The dispersion of the local-field correction is not expected to drastically change the shape of our calculated $\chi^{(2)}$, since $|\epsilon(\omega)| = [\epsilon_1^2(\omega)+\epsilon_2^2(\omega)]^{1/2}$ averages out the strong variations of $\epsilon_1(\omega)$ and $\epsilon_2(\omega)$. Only the ω resonance of L-Λ structure may be slightly enhanced because of the corresponding peak in $\epsilon(\omega)$.

As we have seen in Figs. 3, 5, and 7, the structures in $|\chi_{14}^{(2)}(2\omega)|$ are closely related to the ones in $\epsilon_2(\omega)$. Therefore, it may be possible to predict the nonlinear optical spectrum of a crystal simply from the linear spectrum, without resorting to the details of the band structure and the use of Eq. (2). In the following, we suggest a simple scheme to accomplish this objective. The calculation in-

TABLE VII. Summary of parameters used in Eq. (5).

$\hbar\omega_1$ (E_0), $\hbar\gamma_1$	0.46, 0.05 eV	$A_1=0.08$
$\hbar\omega_2$ ($E_0+\Delta_0$), $\hbar\gamma_2$	0.64, 0.01	$A_2=0.006$
$\hbar\omega_3$ (E_1), $\hbar\gamma_3$	2.58, 0.025	$A_3=0.69$
$\hbar\omega_4$ ($E_1+\Delta_1$), $\hbar\gamma_4$	2.8, 0.15	$A_4=5.14$
$\hbar\omega_5$ (E_2), $\hbar\gamma_5$	4.7, 0.15	$A_5=10.34$
$\hbar\omega_6$, $\hbar\gamma_6$	4.4, 0.02	$A_6=0.38$
$\hbar\omega_7$, $\hbar\gamma_7$	4.58, 0.01	$A_7=0.06$
$\hbar\omega_8$, $\hbar\gamma_8$	6.12, 0.01	$A_8=0.003$
$\hbar\omega_9$, $\hbar\gamma_9$	6.34, 0.01	$A_9=0.01$
$\hbar\omega_{10}$, $\hbar\gamma_{10}$	6.8, 0.01	$A_{10}=0.06$

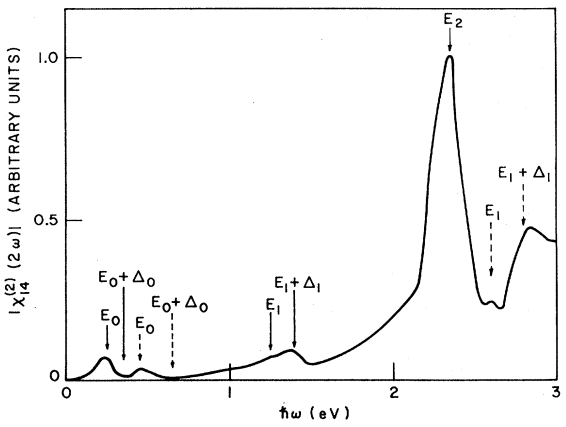

FIG. 8. $|\chi_{14}^{(2)}(2\omega)|$ calculated from Eq. (5).

volves two steps:

(a) *Approximating the linear spectrum,* $\epsilon_2(\omega)$. The simplest way is to approximate the structures in $\epsilon_2(\omega)$ by a set of Lorentzian lines with proper strength and linewidths:

$$\epsilon_2^a(\omega) = \sum_{\alpha=1}^{10} \frac{A_\alpha \gamma_\alpha/\pi}{(\omega-\omega_\alpha)^2+\gamma_\alpha^2} . \tag{4}$$

Let us take the III–V compounds as an example. We can use $\alpha = 1-5$ to approximate the five peaks E_0, $E_0+\Delta_0$, E_1, $E_1+\Delta_1$, and E_2, in the linear $\epsilon_2(\omega)$ spectrum. Except $E_0+\Delta_0$, which is from $2\rightarrow 5$ (2nd band $\rightarrow$ 5th band in Fig. 1) transitions, these peaks are mainly due to $3\rightarrow 5$ and $4\rightarrow 5$ transitions. The lines labeled by $\alpha = 6-10$ are used to approximate the transitions from the same valence bands to the 6th conduction band in the same $\vec{k}$ regions as those transitions responsible for the $\alpha = 1-5$ peaks.

(b) *Approximating* $|\chi_{14}^{(2)}(2\omega)|$. In principle, one can calculate $|\chi_{14}^{(2)}(2\omega)|$ by considering all possible transitions among the ten lines. However, in order to be consistent with the interband transitions in Eq. (2), we do not allow transitions between states in different regions of the Brillouin zone. Therefore, the approximated form of $\chi_{14}^{(2)}(2\omega)$ for a III–V compound is given by

$$\chi_{14}^{(2)}(2\omega) = C\sum_{\alpha=1}^{5}\left(\frac{1}{(\omega-\omega_\alpha-i\gamma_\alpha)(2\omega-\omega_{\alpha+5}-i\gamma_{\alpha+5})}+\frac{1}{(2\omega-\omega_\alpha-i\gamma_\alpha)(\omega-\omega_{\alpha+5}-i\gamma_{\alpha+5})}\right.$$
$$\left.+\frac{1}{(\omega-\omega_\alpha-i\gamma_\alpha)(\omega+\omega_{\alpha+5}+i\gamma_{\alpha+5})}+\frac{1}{(\omega+\omega_\alpha+i\gamma_\alpha)(\omega_\alpha-\omega_{\alpha+5}-i\gamma_{\alpha+5})}\right) A_\alpha A_{\alpha+5} , \tag{5}$$

where C is a constant which accounts for the strengths of the $5\rightarrow 6$ transitions. In Eq. (5), we have neglected the nonresonant terms, since they contribute to the background only.

We have applied Eqs. (4) and (5) to InAs. The parameters ω_α, A_α, and γ_α in which $\alpha = 1-7$, which reproduce the main peaks E_0 to E_2 of the theoretical $\epsilon_2(\omega)$ in Ref. 17 to within 7%, are listed in Table VII. ω_8 to ω_{10} were determined from the band structure of InAs given in Ref. 17. The other parameters were determined by requiring the $\epsilon_2(\omega)$ in Eq. (4) to be a monotonically decreasing function of ω for $\hbar\omega > 5$ eV. Therefore, they were not uniquely determined. However, the $\chi_{14}^{(2)}(2\omega)$ in the range of interest is not very sensitive to the choice of these parameters. The structure at 6.1 eV in the $\epsilon_2(\omega)$ of Ref. 17 is not accounted for because it comes from $4\rightarrow 7$ transitions. The resultant $|\chi_{14}^{(2)}(2\omega)|$ is plotted in Fig. 8. Again, we use solid arrows to indicate structures associated with the 2ω resonances of the lines, and dashed arrows for the ω resonance of the lines themselves. The resolution of the calculation is 0.05 eV. Except for the line shapes above 2.4 eV, the agreement between the results in Figs. 5 and 8 is fairly good.

V. SUMMARY

We have calculated $|\chi_{14}^{(2)}(2\omega)|$ with either constant or $\vec{k}$-dependent matrix elements. The results are compared with the ones obtained by Bell[15] and show definite improvement. The $|\chi_{14}^{(2)}(2\omega)|$ calculated with $\vec{k}$-dependent matrix elements agrees better with the experimental data. Two structures in $|\chi_{14}^{(2)}(2\omega)|$ of InSb have been identified as due to double resonances. One of them can possibly account for the structure at 1.6 eV observed by Chang *et al.*[1] The limiting values of $|\chi_{14}^{(2)}(2\omega|$ as $\omega\rightarrow 0$ in our calculations are smaller than the measured values by an order of magnitude. This is presumably because the local-field correction has not been included in the calculations.

The strong correlations between the structures in the linear optical spectrum and the nonlinear susceptibility suggest that it may be possible to find $|\chi_{14}^{(2)}(2\omega)|$ approximately from a simple atomlike model. We have considered such a model and applied it to InAs as an example.

Several conclusions can be made from the present studies: (a) Except those due to double resonances, structures in $\chi_{14}^{(2)}(2\omega)$ are closely related to the ones in the linear optical spectrum. (b) Double resonances which exist in the case of InSb do not appear in GaAs and InAs. One expects to find double resonances only in crystals with the appropriate band structures. (c) The $\vec{k}$-dependent matrix elements play an important role in determining the nonlinear optical properties of solids. The interference effect shown in the case of InSb provides an illuminating example which does not happen in the linear case. (d) The local-field effect is important in the evaluation of the absolute magnitude of $|\chi_{14}^{(2)}(2\omega)|$. (e) The nonlinear optical spectrum $|\chi_{14}^{(2)}(2\omega)|$ is much more sensitive to the details of the band structure and transition matrix elements than to the linear optical spectrum $\epsilon(\omega)$.

ACKNOWLEDGMENTS

We would like to thank Professor Marvin L. Cohen and D. J. Chadi for providing the spin-orbit program for the calculations.

†Work supported in part by U. S. Energy Research and Development Administration and Research Committee at University of California, Davis.
*Research sponsored by the Air Force Office of Scientific Research, Air Force Systems Command, USAF, under Grant No. AFOSR-72-2353.
‡Research supported by U. S. Energy Research and Development Administration.

[1]R. K. Chang, J. Ducuing, and N. Bloembergen, Phys. Rev. Lett. 15, 415 (1965).
[2]F. G. Parsons and R. K. Chang, Opt. Commun. 3, 173 (1971).
[3]H. Lotem, G. Koren and Y. Yacoby, Phys. Rev. B 9, 3532 (1974).
[4]D. Bethune, A. J. Schmidt, and Y. R. Shen, Bull. Am. Phys. Soc. 18, 1577 (1973); Phys. Rev. B 11, 3867 (1975).
[5]J. A. Armstrong, N. Bloembergen, J. Ducuing, and P. S. Pershan, Phys. Rev. 127, 1918 (1962).
[6]R. Loudon, Proc. Phys. Soc. Lond. 80, 952 (1962).
[7]P. N. Butcher and T. P. McLean, Proc. Phys. Soc. Lond. 81, 219 (1963); 83, 579 (1964).
[8]P. L. Kelley, J. Phys. Chem. Solids, 24, 607 (1963); 24, 1113 (1963).
[9]H. Cheng and P. B. Miller, Phys. Rev. 143, A683 (1964).
[10]B. F. Levine, Phys. Rev. Lett. 22, 787 (1969).
[11]J. C. Phillips and J. A. Van Vechten, Phys. Rev. 183, 709 (1969).
[12]J. A. Van Vechten, Phys. Rev. 182, 891 (1968).
[13]J. C. Phillips, Phys. Rev. Lett. 20, 550 (1968).
[14]N. Bloembergen, R. K. Chang, and J. Ducuing, in *Physics of Quantum Electronics*, edited by P. L. Kelley, B. Lax and P. E. Tannenwald, (McGraw-Hill, New York, 1966), p. 67.
[15]M. I. Bell, Proceedings of the Conference on the Electronic Density of States, Gaithersburg, Maryland, 1969 (unpublished).
[16]R. R. L. Zucca, J. P. Walter, Y. R. Shen, and M. L. Cohen, Solid State Commun. 8, 627 (1970).
[17]C. V. deAlvarez, J. P. Walter, R. W. Boyd, and M. L. Cohen, J. Phys. Chem. Solids 34, 337 (1973).
[18]D. E. Aspnes (unpublished).
[19]W. Saslow, T. K. Bergstresser, C. Y. Fong, M. L. Cohen, and D. Brust, Solid State Commun. 5, 167 (1967).
[20]J. J. Wynne, Phys. Rev. Lett. 27, 17 (1971).
[21]J. J. Wynne and N. Bloembergen, Phys. Rev. 188, 1211 (1969).
[22]C. Flytzanis and J. Ducuing, Phys. Lett. 26 A315, (1968); Phys. Rev. 178, 1218 (1969).
[23]N. Bloembergen, *Nonlinear Optics* (Benjamin, New York, 1965), p. 69.
[24]We are grateful to J. R. Chelikowsky for providing part of this information.